Crustal-Scale Thermal Models: Revisiting the Influence of Deep Boundary Conditions

Denise Degen[1], Karen Veroy[2,3], Magdalena Scheck-Wenderoth[4,5], Florian Wellmann[1]

[1]Computational Geoscience and Reservoir Engineering (CGRE), RWTH Aachen University, Wüllnerstraße 2, 52072 Aachen, Germany
[2]Centre for Analysis, Scientific Computing and Applications, Department of Mathematics & Computer Science, Eindhoven University of Technology (TU/e), Groene Loper 5, Eindhoven, The Netherlands
[3]Faculty of Civil Engineering, RWTH Aachen University, Schinkelstraße 2, Aachen, Germany
[4]Faculty of Georesources and Materials Engineering, RWTH Aachen University, Aachen, Germany
[5]GFZ German Research Centre for Geosciences, Telegrafenberg, 14473 Potsdam, Germany

Key Points:

- We demonstrate that basin-scale models with a low vertical extent are boundary-dominated.
- In boundary-dominated models, the boundary settings dominate over other. thermal parameter.
- The influence of the boundary condition is only apparent through a global sensitivity analysis.

Corresponding author: Denise Degen, `denise.degen@cgre.rwth-aachen.de`

Abstract

The societal importance of geothermal energy is significantly increasing because of its low carbon-dioxide footprint. However, geothermal exploration is also subject to high risks. For a better assessment of these risks, extensive parameter studies are required that improve our understanding of the subsurface. This yields computationally demanding analyses. Often this is compensated by constructing models with a low vertical extent. In this paper, we demonstrate that this leads to entirely boundary-dominated and hence uninformative models. We demonstrate the indispensable requirement to construct models with a large vertical extent to obtain informative models with respect to the model parameters. For this quantitative investigation, global sensitivity studies are essential since they also consider parameter correlations. To compensate for the computationally demanding nature of the analyses, we employ a physics-based machine learning approach, namely the reduced basis method, instead of reducing the physical dimensionality of the model. The reduced basis method yields a significant cost reduction while preserving the physics and a high accuracy, thus providing a more efficient alternative to considering, for instance, a lower vertical extent. The reduction of the mathematical instead of physical space leads to less restrictive models and, hence, maintains the model prediction capabilities. We use this combination of methods for a detailed investigation of the influence of model boundary settings in typical regional-scale geothermal simulations and highlight potential problems.

1 Introduction

Geothermal energy is an important part of the future energy mix on the path to a more sustainable use of resources. Many aspects influence the potential use of a geothermal resource, with one prime parameter being the temperature in the subsurface. In order to determine expected temperatures on a regional scale, geothermal simulations are often performed (Gelet et al., 2012; Kohl et al., 1995; O'Sullivan et al., 2001; Taron et al., 2009; Watanabe et al., 2010). A common procedure is to start with a geological model, representing the main geological sequences, grouped by similar thermal properties, and to use this information for the parameterization of a geothermal simulation (Cacace et al., 2010; Mottaghy et al., 2011a; Sippel et al., 2015). However, the (effective) thermal parameters of subsurface geological units (e.g. thermal conductivity, heat production rate) are generally uncertain and the material parameters are therefore often calibrated on the basis of temperature observations.

Extensive parameter studies or full uncertainty quantification studies are non-trivial since basin-scale models tend to be computationally demanding. To overcome this issue, a common approach is to generate models that have a large horizontal extension but a very low vertical extent (Pribnow & Schellschmidt, 2000; Pribnow & Clauser, 2000; Mottaghy et al., 2011b; Vogt et al., 2013; Kastner et al., 2015). The boundary conditions for these models are either based on best estimates or retrieved from larger models (Noack et al., 2013). We investigate here in detail how these typical approaches to treat boundary conditions influence all subsequent analyses, leading partly to fully boundary-dominated models. Here, we demonstrate that they only have very limited capabilities for the analysis and understanding of the physical processes. During the model calibration, we can compensate for possible boundary errors through an adjustment of the thermal properties. Meaning that this has no direct impact on the temperature distribution but a significant impact on the physical plausibility of our model. Hence, for scenarios that lay outside of our calibrated regime, we lose any prediction capabilities. This is a major restriction when considering the sparse nature of our observations.

In order to investigate the influence of thermal boundaries, we employ full global sensitivity analyses (SA) for several case studies. These types of global SA approaches are usually not performed due to the high associated computational cost. To address this computational challenges, we are replacing a full finite element solution of our forward solves with the reduced basis solution. This approach aims to reduce the complexity of the mathematical instead of physical space, yielding fast, accurate, and physics-preserving surrogate models. With these surrogate models, we then perform the global sensitivity analyses on several model realizations of a regional-scale geothermal basin model in northern Germany (around Berlin and the state of Brandenburg) to demonstrate the influence of the lower boundary condition on the simulation.

Additionally, we perform an automated model calibration to provide an objective and reproducible way to compensate for the errors of both the physical and geological model. Sensitivity analysis for basin-scale models have been performed before in Noack et al. (2012) and also been combined with automated model calibrations (Wellmann & Reid, 2014). Also, Fuchs and Balling (2016) consider model calibrations but in their case without sensitivity analyses. Furthermore, local sensitivity studies are presented in Ebigbo et al. (2016). However, none of these can address the computationally demanding nature of the problem. Therefore, they are limited in the number of parameters, sensitivity analyses, and model calibrations they can perform. By using a physics-based machine learning approach instead of the finite element method, we can reduce the compute time of the forward solve by several orders of magnitude. It allows, in turn, to perform global sensitivity analysis and full flexibility in the model calibration.

Global sensitivity analyses have been performed for hydrological problems (van Griensven et al., 2006; Tang et al., 2007; Cloke et al., 2008; Zhan et al., 2013; Baroni & Tarantola, 2014; Song et al., 2015), for volcanic source modeling (Cannavó, 2012), and for geothermal heat exchangers (Fernández et al., 2017). In Degen, Veroy, Freymark, et al. (2020), the authors have investigated the influence of both local and global sensitivity studies for the Upper Rhine Graben. In this paper, we want to use the combination of the global sensitivity study and model calibration, as presented in Degen, Veroy, Freymark, et al. (2020), to investigate the influence of the placement of the boundaries on the model predictions.

The paper is structured as follows: We present the methodologies and the governing equations. In Section 2 and in Section 3, we conceptually introduce the problem of the lower boundary condition using a simple 1D model. Section 4 presents the impact of the lower boundary conditions, by focusing on a real-case basin-scale application. Therefore, we present and discuss the results of both global sensitivity analyses and model calibrations.

2 Materials and Methods

In the following, we will briefly describe the geothermal conduction problem used for the forward simulations of the temperature. Furthermore, we introduce the concept of sensitivity analyses.

2.1 Physical Model

For the simulation of the temperature field, we are considering a geothermal conduction problem with the radiogenic heat production S as the source term after Bayer et al. (1997):

$$\lambda \nabla^2 T + S = 0, \tag{1}$$

where λ is the thermal conductivity, and T the temperature. Nondimensionalizing the problem, for efficiency reasons and to investigate the relative importance, leads to eq. 2:

$$\frac{\lambda}{\lambda_{\text{ref}}\ S_{\text{ref}}}\ \frac{\nabla^2}{l_{\text{ref}}^2}\ (\frac{T - T_{\text{ref}}}{T_{\text{ref}}})\ +\ \frac{S}{S_{\text{ref}}\ T_{\text{ref}}\ \lambda_{\text{ref}}}\ =\ 0. \tag{2}$$

Here, λ_{ref} is the reference temperature, T_{ref} the reference temperature, S_{ref} the reference radiogenic heat production, and l_{ref} the reference length. Note that the Laplace operator (∇) is used on the nondimensional space. For the motivational study we neglect the radiogenic heat production to focus the analysis on the heat diffusion and the boundary condition. Furthermore, we apply for all models Dirichlet boundary conditions at the top and bottom of the model domain.

2.2 Sensitivity Analysis

Sensitivity analyses aim to determine which model parameters influence the model response to what extent. So, in our studies, we want to investigate, which thermal conductivities and radiogenic heat productions have a significant impact on the temperature distribution. We distinguish two types of sensitivity analyses: local and global ones. Local sensitivity analyses consider that all parameters are independent of each other. In contrast, global sensitivity studies investigate also the parameter correlations. A detailed comparison of both methods for hydro-geological problems is presented in Wainwright et al. (2014) and for basin-scale geothermal application in Degen, Veroy, Freymark, et al. (2020).

For the sensitivity analysis (SA), we need to define a quantity of interest. We use the L2-norm of the temperature misfit to the reference model as our quantity of interest, for the motivational. The quantity of interest for the real-case model is the L2-norm of the temperature misfit between the simulated and observed temperature values.

For the global sensitivity analysis, we are using the Sobol method with the Saltelli sampler, this is a variance-based sensitivity analysis operating in a probabilistic framework. Further information regarding the Sobol method can be found in Sobol (2001);

Saltelli (2002); Saltelli et al. (2010). For the sensitivity analyses, we are using the python library SALib (Herman & Usher, 2017).

2.3 Model Calibration

The main aim of this paper is to investigate the influence of the lower boundary condition on our physical interpretation through an evaluation of the temperature distribution. This the reason why we make use of global sensitivity analyses. However, in practical applications, we often want to calibrate our model against existing temperature measurements to ensure the correctness of the model.

For this, we require model calibrations, which aim to compensate for existing model errors by an adjustment of the model parameters. For deep geothermal applications calibrations are challenging since we usually have only a few shallow data points (Degen, Veroy, Freymark, et al., 2020). As we will see for the real-case study, it is possible to adjust a given model to the observed temperatures. However, larger model errors yield unphysical model parameters, imposing the danger of losing the predictability for observation points that have not been included in the calibration. This aspect will be discussed in detail later on.

In this work, we employ a trust region reflective algorithm as the calibration method, which is a suitable choice for constrained problems, meaning that we have defined ranges for our thermal parameters (Branch et al., 1999). During the calibration, we minimize the L1 norm of the misfit between the simulated and observed temperature measurements. We consider the L1 norm to put less weight on outliers. The analysis is performed through the python library SciPy (Virtanen et al., 2020). For more details regarding the method, we refer to Branch et al. (1999) and more details regarding the application to basin-scale models we refer to Degen, Veroy, Freymark, et al. (2020).

3 Motivational Example

In this paper, we investigate the influence of the impact of the lower boundary condition on the temperature distribution. This is an issue concerning geological models in general. For this reason, we first demonstrate the problem using a highly simplified motivational model. This motivational study aims to illustrate the general problems and not to represent a realistic geothermal application. To demonstrate that the issue has a major impact on real-case geothermal applications, we extend the investigation to the real-case study of Berlin-Brandenburg (a sedimentary basin in north-eastern Germany which is introduced in Section 4).

3.1 Forward Model

We first introduce the forward problem used for the motivational study, for which we consider a simplified 1D model. The 3-layer model, schematically shown in Fig. 1,

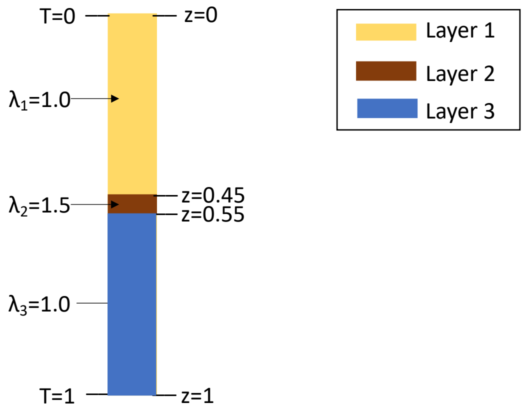

Figure 1. Schematic representation of the 3-layer 1D model used for the motivational study of the boundary condition problem. The depth is denoted with z, the temperature with T, and the thermal conductivity with λ.

consists of three layers, where the middle layer is thinner than both adjacent layers. Furthermore, the thermal conductivity of all layers is 1.0. We chose a thermal conductivity of 1.0 for the top and bottom layer and a thermal conductivity of 1.5 for the thin layer. At the top of the model, we apply a Dirichlet boundary condition of zero for the temperature and at the bottom a Dirichlet boundary condition of one. We solve the model analytically. Note that we consider the nondimensional form to focus the analysis on the relative difference.

In the following analyses, we analyze the influence of the thermal conductivity of the thin middle layer (Layer 2 in Fig. 1) with respect to its distance from the boundary conditions. Therefore, we change the position of the thin layer. Three different positions of the thin layer are considered: i) the thin layer adjacent to the base boundary condition (position P1 in Fig. 2), ii) the thin layer in the center of the model (position

P2 in Fig. 2), and iii) the thin layer adjacent to the top boundary condition (position P3 in Fig. 2). For the sensitivity analysis, we define the scenario P2 as the reference model, where the thin layer is located around the center (see Fig. 1). Consequently, the reference model represents the case of the lowest possible boundary influence.

3.2 Impact of the Boundary Condition

To determine the influence of the lower boundary condition, we perform a global sensitivity analysis with 100 equally spaced temperature measurements in depth ranging from zero to one. Furthermore, we allow a variation range of ± 50 % for the thermal conductivities of all three layers.

The results of the global SA are shown in Fig. 2. Before discussing the results for this SA, we want to specify the terminology. In Fig. 2 we obtain first- and total-order terms. The first-order terms describe the influence from the parameter itself, whereas the total-order term describes the influence from the parameter plus any parameter correlations. Consequently, the correlation is defined as the difference between the total- and first-order contributions. We want to investigate the influence of both boundary conditions on the model. Therefore, we need to take the scenario, where the thin layer is in the center of the model (P2) as the reference case. This means that high influences of the parameters correspond to a high boundary dominance.

For our simple model, all thermal conductivities are dominated by total-order contributions for all three scenarios (P1-P3). This means that we have high parameter correlations. The high correlations are induced by the set-up of the model, where the temperature distribution is only determined by the two Dirichlet boundary conditions and by the ratio of the thermal conductivities between adjacent layers. Furthermore, the influence of λ_2 is at all three positions the lowest, which is an effect of the lower thickness of this layer. Also note that for λ_2, we observe nearly no first-order influences.

Focusing on scenario P1, we obtain the highest boundary dominance for λ_1, which is situated at the upper boundary condition. The lowest influence is obtained for λ_2 because of the above-described reason. λ_3 has a significantly lower influence of the boundary than λ_1, which is logical since it is further away from the boundary. Interesting is that the decrease in the first-order contributions is more pronounced than the decrease in the total-order contributions. This shows that the remaining boundary influences are mainly arising from parameter correlations. By having a detailed look at the SA, we observe that the main correlations are arising from the correlation between λ_1 and λ_3. For scenario P3, we observe the same behavior with reversed roles for λ_1 and λ_3. For scenario P2, we obtain a boundary dominance of λ_1 and λ_3, which are both adjacent to the boundaries. λ_2 is situated in the center of the model, resulting in negligible contributions.

The results for all three scenarios are following our expectations since we obtain the smallest boundary influences if the layers are further away from the boundaries. Note

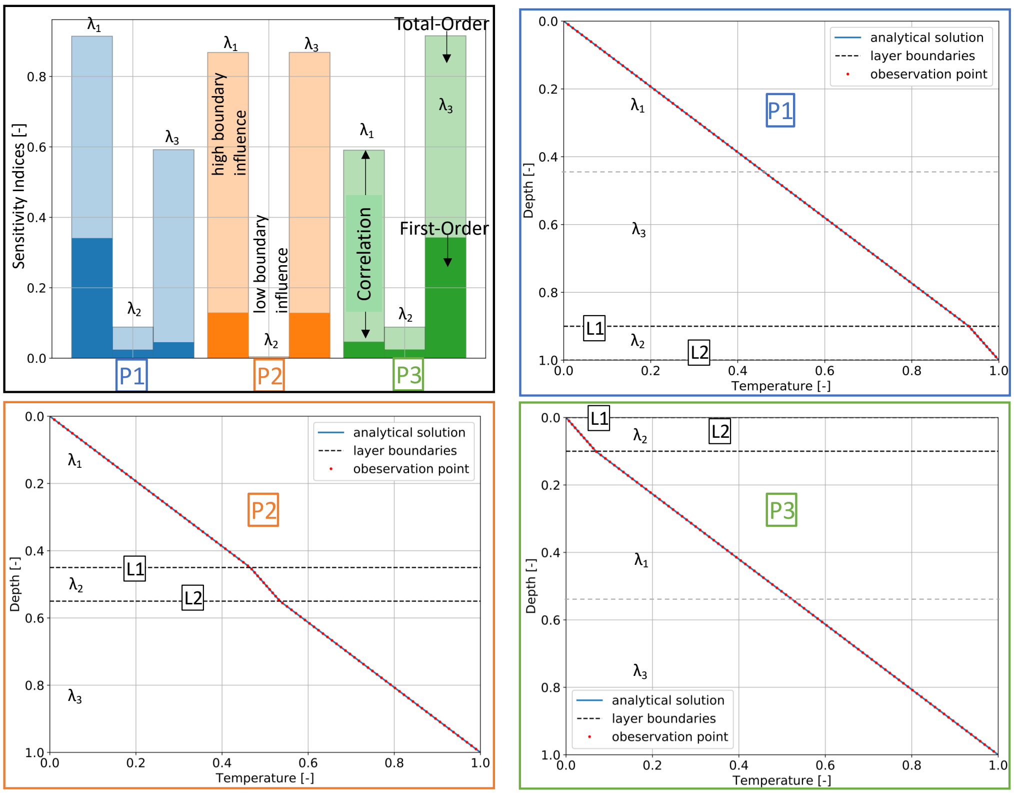

Figure 2. Black Box: First- and total-order Sobol sensitivity indices of the thermal conductivities for the 3-layer model with respect to the distance from the boundaries. Blue Box: Scenarios P1, where the thin layer is adjacent to the bottom model boundary. Orange Box: Scenarios P2, where the thin layer is in the middle of the model boundary. Green Box: Scenarios P3, where the thin layer is adjacent to the top model boundary. Note that the interfaces of the thin layer are denoted with L.

that these results can only be returned by a global SA. A local SA would assume that the influence is coming from the parameter itself. As an example, in P1 this would lead to a significant overestimation of the influence of λ_3. In the worst case, this yields the misleading conclusion that λ_3 is still greatly influenced by the boundary.

To conclude, for our motivational example we lose the information about the thin layer when it approaches the boundary condition. Or, as an alternative viewpoint, these two examples highlight the strong influence of boundary conditions on the simulation results. In a typical geothermal simulation setting, the position of the top boundary condition is usually defined as the land surface and cannot be changed. Its impact and possible ways to solve the issue have been discussed in Degen, Veroy, and Wellmann (2020b). In contrast, the position of the lower boundary condition is usually adjustable.

4 Case Study Berlin-Brandenburg

After demonstrating the general problem of the placement of the boundary for geological models, we want to show the consequences for real-case studies. Therefore, we exchange our simplified 1D example with various representations of the Berlin-Brandenburg model, which cover a sedimentary basin in north-eastern Germany (see Fig. 3).

4.1 Berlin-Brandenburg Models

In this paper, we are using three different versions of the Berlin-Brandenburg (BB) model. The first version, from now on denoted as the Berlin-Brandenburg LAB model (BB-LAB), has already been presented in Noack et al. (2012) and can be seen in Figure 3a. It has an extension of 250 km in the x- and of 210 km in the y-direction and extends down to the lithosphere–asthenosphere boundary (LAB). The model consists of 15 lithological units and the mesh consists of deformed eight-noded prisms. The grid resolution is one km in the horizontal directions, whereas the vertical length of the layers corresponds to the vertical element length, resulting in a mesh with 840,000 degrees of freedom.

The second model, in the following, referred to as the Berlin-Brandenburg 6 km model, or BB-6km (Figure 3b), has the same horizontal extent but extends to a depth of 6 km instead of down to the LAB. It is presented in Noack et al. (2013) and consists of 12 lithological units. The model is discretized into a tetrahedral mesh. In comparison to the Brandenburg LAB model, it is refined in both geological and grid resolution terms. We have a horizontal element resolution of 0.22 km^2 and a vertical resolution that is interpolated from the z-evaluations of the geological layers with a minimum thickness of 0.1 m, resulting in a mesh of 1,546,675 degrees of freedom.

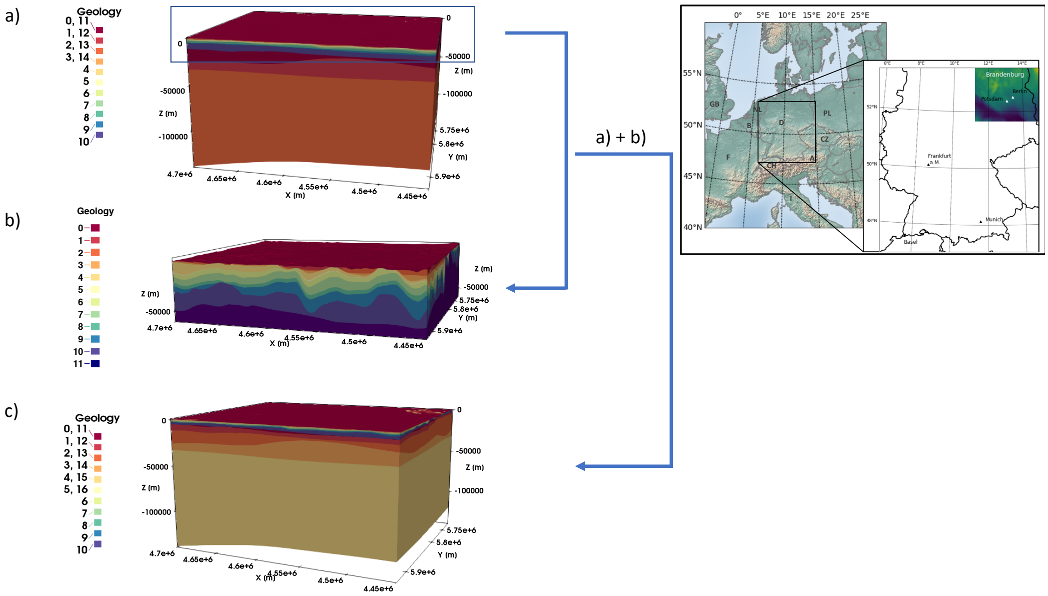

Figure 3. Geology of the a) Berlin-Brandenburg LAB model, b) Berlin-Brandenburg 6 km model, and the c) Berlin-Brandenburg combined model. For the acronyms, we refer to Table S1.

Combining the Berlin-Brandenburg 6 km model, the Berlin-Brandenburg LAB model, and removing the minimal vertical thickness of 0.1 m results in the third version of the Brandenburg model, denoted as the Berlin-Brandenburg combined model, or BB-combined (Figure 3c). Consequently, this model consists of 17 geological layers, where the upper 11 layers have the same resolution as in the BB-6km model. The lower six layers have the same vertical resolution as the BB-LAB model and the same horizontal resolution as the Berlin-Brandenburg 6 km model. This results in a tetrahedral mesh with 2,141,550 degrees of freedom.

For both the BB-LAB and BB-combined model, we apply a Dirichlet boundary condition of 8 ˚C, corresponding to the average annual temperature, at the top of the model. Moreover, we set a Dirichlet boundary condition of 1300 ˚C at the base of the LAB (Turcotte & Schubert, 2002). Additionally, we allow a scaling of this boundary condition of ± 10 % to account for errors in the geometrical description of the LAB. The Berlin-Brandenburg 6 km model has the same upper boundary condition, but at the bottom, we use various Dirichlet boundary conditions directly taken from the Berlin-Brandenburg LAB model. Furthermore, we consider a lower boundary conditions derived by Kriging. For this interpolation, we consider 900 equally spaced temperature observation from the BB-LAB model in a depth of 6 km and derive the interpolated boundary with a spherical variogram. All thermal properties are summarized in Table S1. The forward simulations are performed using the DwarfElephant package (Degen, Veroy, & Wellmann, 2020a) with a linear and nonlinear solver tolerance of 10^{-10}. Due to the nondimensional nature of the problem, no preconditioners are needed for the finite element evaluations.

We set the reference thermal conductivity λ_{ref} to the maximum thermal conductivity of the BB-LAB model of 3.95 W m^{-1} K^{-1}. For the BB-LAB and the BB-combined model, the maximum temperature of 1300 °C is the reference temperature T_{ref}, whereas for the BB-6km model a reference temperature of 8 °C is chosen. Homogeneous Dirichlet boundary conditions are used to achieve a better performance of the numerical methods (Degen, Veroy, & Wellmann, 2020a). The Berlin-Brandenburg 6 km model has a constant Dirichlet boundary condition at the top. At the bottom, the model has a Dirichlet boundary condition with a different temperature value for each element. We set the top boundary condition to zero by using the value of the top boundary as our reference parameter. The bottom boundary condition is set to zero via a lifting function. In case of the Berlin-Brandenburg LAB and combined model, we have constant Dirichlet boundary conditions values for both upper and lower boundary, and hence we can use both of them as our reference parameter. We chose the value of the lower boundary condition to better reduce the magnitude of the temperatures, which yields a better performance. The maximum radiogenic heat production of the BB-LAB model of 2.5 μW m^3 is the reference radiogenic heat production S_{ref}. The reference length l_{ref} corresponds to the maximum x-extent of all models (250,000 m).

For the validation of the models we use temperature measurements presented in Noack et al. (2012, 2013) and based on Förster (2001). The temperature consists of 81 temperature measurements from 44 wells in the area of Brandenburg. It has been measured at various depth and stratigraphic levels.

4.1.1 Reduced Models

The reduced basis (RB) method is a model order reduction technique that aims to significantly reduce the dimensionality of problems resulting from a discretization (e.g. via finite elements) of parameterized partial differential equations (PDE). The method is decomposed into an offline and online stage, where the offline stage, being a one time cost, constructs a reduced basis, and therefore compromises all expensive pre-computations.

The online stage uses this reduced basis to allow very fast forward evaluations, typically in the range of a few milliseconds (Degen, Veroy, & Wellmann, 2020a). In contrast to other surrogate models, the RB method has the advantage that temperatures can be extracted at every location of the model and not only at predefined points. Furthermore, for geothermal conduction problems, it provides an error bound, enabling an objective evaluation of the approximation quality.

For further information regarding the RB method we refer to Prud'homme et al. (2002); Veroy et al. (2003); Hesthaven et al. (2016) and for further information in the context of geosciences we refer to Degen, Veroy, and Wellmann (2020a).

For using the RB method, we decompose our geothermal problem into a parameter-dependent and -independent part. In the following, we define the affine decompositions of the integral formulation of the PDE for the various scenarios of the Brandenburg model. Note that we use the operator representation. Therefore, we talk about the bilinear form instead of the stiffness matrix, and the linear form instead of the load vector.

For all Berlin-Brandenburg models, the bilinear form a has the following decomposition:

$$a(w, v; \lambda) = -\sum_{q=0}^{n} \lambda_q \int_{\Omega} \nabla w \ \nabla v \ d\Omega, \qquad \forall v, w \in X, \ \forall \lambda \in \mathcal{D}, \tag{3}$$

where $w \in X$ is the trial function, $v \in X$ the test function, "q" denotes the index of the training parameter (for more information see Tab. S1), X the function space ($H_0^1(\Omega) \subset X \subset H_1(\Omega)$), Ω the spatial domain in $\mathbb{R}^3$, $\lambda \in \mathcal{D}$ the parameter, and $\mathcal{D}$ the parameter domain in $\mathbb{R}^n$. We denoted the number of thermal conductivities in the training sample with n. Consequently, n is equal to thirteen, nine, and fourteen for the BB-LAB, BB-6km, and BB-combined model, respectively.

For all Berlin-Brandenburg models, except the BB-6km model with a lower boundary condition derived via Kriging, the linear form f is decomposed in the following way:

$$f(v; \lambda, s) = -\sum_{q=0}^{n} \lambda_q \ s \int_{\Gamma} \nabla v \ g(x, y, z) \ d\Gamma + \ s \int_{\Gamma} \nabla v \ S \ d\Gamma, \qquad \forall v \in X, \ \forall \lambda \in \mathcal{D}, \tag{4}$$
$$\text{with } g(x, y, z) = T_{\text{top}} \frac{h(x, y, z) - z_{\text{bottom}}(x, y)}{d(x, y)}.$$

Here, Γ is the boundary in $\mathbb{R}^3$, s the scaling parameter for the lower boundary condition, $g(x, y, z)$ the lifting function, T_{top} the temperature at the top of the model, $h(x, y, z)$ the location in the model, $z_{\text{bottom}}(x, y)$ the depth of the bottom surface, and $d(x, y)$ the distance between the bottom and top surface.

For the BB-6km with a Kriging lower boundary condition, the linear form slightly changes to the following:

$$
\begin{aligned}
f(v; \lambda, s) &= -\sum_{q=0}^{8}\sum_{i=0}^{3} \lambda_q \; s_i \int_\Gamma \nabla v \; g_i(x, y, z) \; d\Gamma + \; s_2 \int_\Gamma \nabla v \; S \; d\Gamma, \quad \forall v \in X, \; \forall \lambda \in \mathcal{D}, \\
\text{with } g_1(x, y, z) &= g_3(x, y, z) = 1 - \frac{h(x, y, z) - z_{\text{bottom}}(x, y)}{d(x, y)}, \\
g_2(x, y, z) &= \left(\frac{3 \; d(x, y)}{2a} - \frac{1}{2}\left(\frac{d(x, y)}{a}\right)^3\right)\left(1 - \frac{h(x, y, z) - z_{\text{bottom}}(x, y)}{d(x, y)}\right).
\end{aligned}
\tag{5}
$$

Here g_1, g_2, and g_3 are again the lifting functions, with s_1 being the nugget, s_2 the partial sill, s_3 the scaling parameter for the mean temperature, and a the range.

4.1.2 Parameterization and Set-Up of the Sensitivity Analysis

The sensitivity analyses are performed with 13 (BB-LAB model – Fig. 3a), 11 (BB-6km model – Fig. 3b), 14 parameters (BB-combined model – Fig. 3c) and with 10,000 realizations for each parameter to reduce the statistical error. Note that for the Berlin-Brandenburg 6 km model we show exemplarily the results using the Kriging lower boundary condition. The results of the sensitivity analyses using the other boundary conditions are analog to the one shown in this manuscript. We only vary thermal conductivities and keep the radiogenic heat productions constant, to reduce the number of parameters within the reduction and all further analyses. We fix the radiogenic heat productions and not the thermal conductivities because their influence on the overall temperature distribution is smaller. We allow a variation of ± 50 % from the initial thermal conductivities. Also, for the nugget and the partial sill, we allow a variation of ± 50 %. For the scaling parameter of the lower boundary of both the Berlin-Brandenburg LAB model and Berlin-Brandenburg combined model we allow a variation ± 10 % and for the scaling parameter of the mean temperature at the lower boundary condition of the BB-6km model ± 20 %, in order to account for the uncertainties related to those boundary conditions.

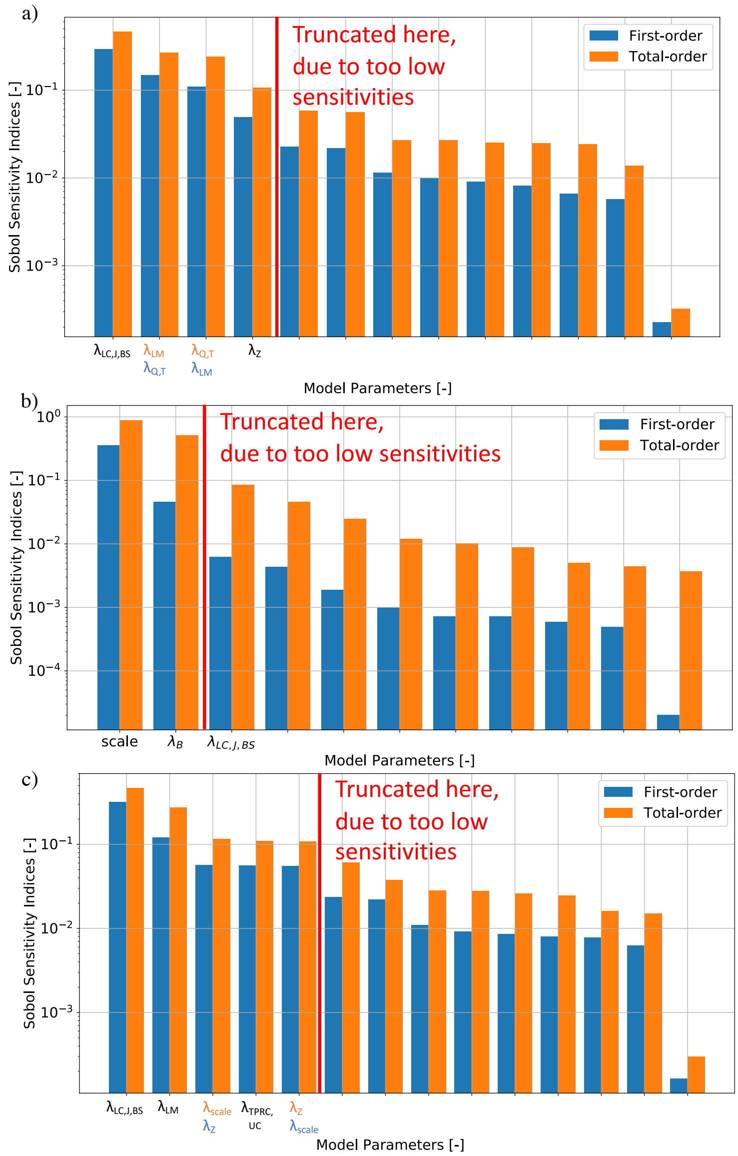

Figure 4. Global Sensitivity analysis for a) the Berlin-Brandenburg LAB, b) Berlin-Brandenburg 6 km model, and c) Berlin-Brandenburg combined model. We show the first- (blue) and total-order contributions (orange). Please refer to Tab. S1, for the acronyms of the thermal conductivities

4.2 Results

As for the conceptual study, we want to demonstrate the influence of the lower boundary condition. Therefore, we first present the results from the sensitivity analysis and then the results from the model calibration.

4.2.1 Sensitivity Analysis

Before presenting the results of the sensitivity analyses, note that all analyses were performed with the aim to investigate the influence of the lower boundary condition. We do not aim to characterize the influences of every single thermal parameter in the model. Nevertheless, some geological impacts can be derived and are presented in the following.

Regarding the sensitivities, the Berlin-Brandenburg LAB (Fig. 4a) is mostly influenced by the Lower Cretaceous/Jurassic/Buntsandstein layer. The first-order sensitivity index is dominant over the higher-order indices. Furthermore, the model is sensitive to the Quaternary/Tertiary layer and the Lithospheric Mantle. For the Quaternary/Tertiary layer, we again have predominantly first-order influences, whereas the Lithospheric Mantle mostly impacts through higher-order contributions. Less pronounced is the influence from the Zechstein layer. The observed influence has similar first- and higher-order contributions. This is counter-intuitive since one would expect a high influence of the Zechstein layer due to its high thermal conductivity and highly variable thickness resulting in significant property contrast. To explain this discrepancy, we take a closer look at the set-up of the sensitivity analysis. In the analysis, we combined layers with equal thermal conductivities. Therefore, the thermal conductivities of the Lower Cretaceous, Jurassic, and Buntsandstein layer are combined. Consequently, the high influence of this layer is originating from this high combined sediment thickness. Keep in mind that the aim of this analysis is to determine the influence of the boundary condition. For determining which individual thermal conductivity has the highest influence a separate analysis is required. The remaining thermal conductivities have minor influences and are therefore disregarded in further analyses.

The Berlin-Brandenburg 6 km model is only influenced by the Basement layer and by the variability of the lower boundary condition (Fig. 4b). The influence of the scaling parameter of the mean temperature is significantly higher than the one from the Basement layer. Higher-order contributions dominate both parameters. Note that the Basement layer has nearly no first-order contributions, whereas the scaling parameter has non-dominant first-order contributions.

For the Berlin-Brandenburg combined model (Fig. 4c), we observe a similar pattern. The highest influences, dominated by first-order contributions, are arising from the

Lower Cretaceous/Jurassic/Buntsandstein layer. The influence of both the Lithospheric Mantle and the scaling parameter of the lower boundary condition increased, but higher-order contributions still dominate both parameters. The Tertiary-pre-Rupelian-clay/Upper Cretaceous, and the Zechstein layers are also influencing on the model and comparable first- and higher-order contributions to each other.

4.2.2 Model Calibration – Temperature Distribution

We take the results from the global sensitivity analysis as an input for the following model calibration. Model calibration is necessary to account for model errors of the Berlin-Brandenburg model. Since the calibrations use the results from the sensitivity analyses, we vary six, two, and six thermal conductivites within the calibration for the Berlin-Brandenburg LAB, Berlin-Brandenburg 6 km, and Berlin-Brandenburg combined model, respectively.

The calibration of the Berlin-Brandenburg 6 km model is challenging because of the lower boundary condition. The conventional way to define this boundary condition is to extract it from the calibrated BB-LAB model and apply it to the BB-6km model, although it is generally not clear that the calibration for the larger model is also valid for the shallower model. To evaluate the influence of different calibration results, we compare the model calibration for the shallow model using the boundary condition from two uncalibrated Brandenburg LAB model versions and various hierarchical model calibrations. For the hierarchical models, we chose either the boundary condition from the calibrated BC or a boundary condition obtained via Kriging as the lower boundary condition.

Therefore, we compare in Figure 5 the model calibrations using various lower boundary conditions of the Berlin-Brandenburg 6 km model. At the top panel, we show the difference at the observation points. The differences between the various methods are comparably small, which is not surprising since the calibration aims to minimize the difference between the simulated and observed temperatures at these locations. However, if we look at the three points (P1 to P3, positions shown in Fig. 6), we observe differences between the various calibrations that can exceed 50 °C. Showing the impact that the choice of the boundary conditions has on the overall model.

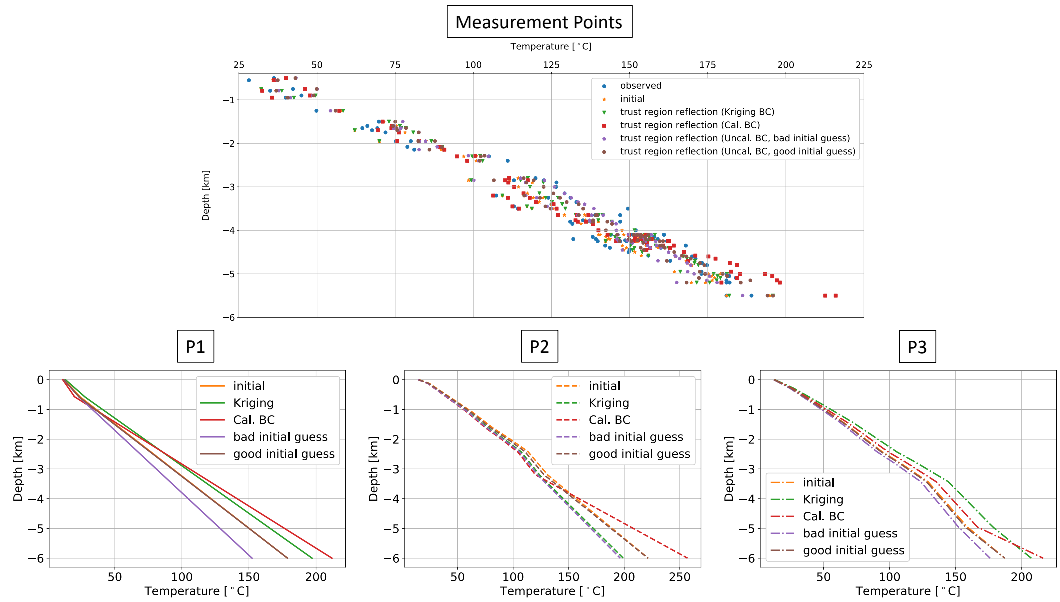

Figure 5. Comparison of the different calibration versions of the Berlin-Brandenburg-6 km model for the observed temperatures at all temperature measurements within the model (top panel) and at three points in the model (bottom panels) The position of the three points P1-P3 are shown in Fig. 6. They where chosen to cover the low temperature, the high temperature, and the by salt structures influenced temperature regions.

We now compare temperature distributions for the interval of the uppermost 6 kilometers of all three versions of the Berlin-Brandenburg model in Fig. 6. For the BB-6km model, we only show exemplarily the hierarchical model calibration. The differences for all three points (P1 to P3) are comparable among the models. Note that the possible variation range of the BB-6km is much larger since the determination of the lower boundary condition is uncertain (see Fig. 5). The BB-LAB and BB-combined model already show the maximum possible variation, whereas the BB-6km model shows only the maximum variation range of the good-fit model.

Lastly, in Fig. 7 we show the differences in the temperature distributions at the three points (P1 to P3) for the entire depth of the BB-LAB and BB-combined models. The major difference between both models is induced by the different treatments of the boundary condition. During the sensitivity analysis of the BB-LAB model, the scaling parameter of the lower boundary condition did not significantly influence the model response, contrary to the analysis of the BB-combined model. Therefore, we consider in the latter model the scaling parameter in the calibration, wheres we keep the value con-

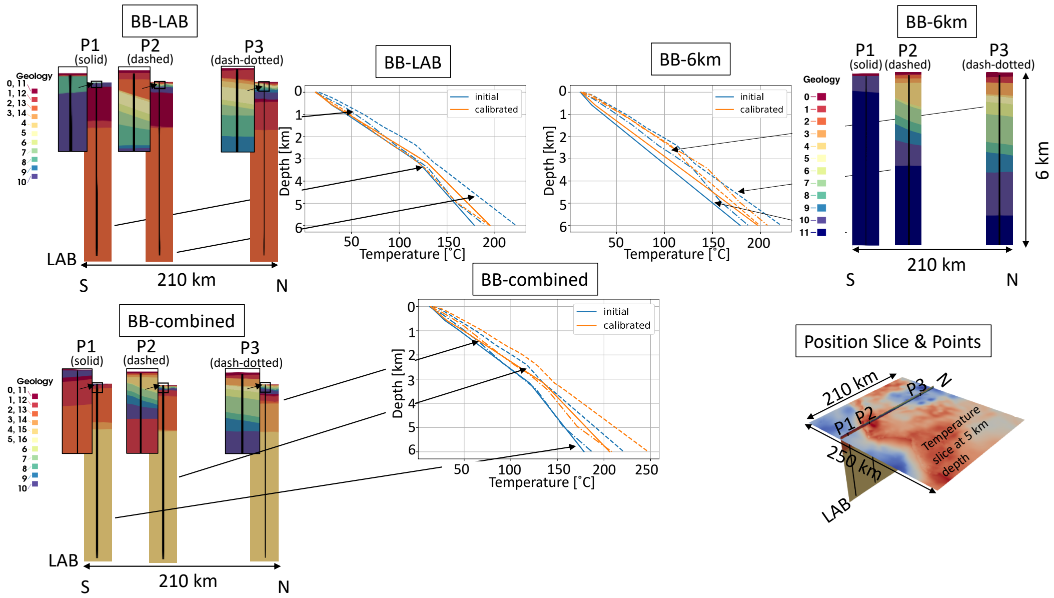

Figure 6. Comparison of the temperature distribution over an interval of 6 km depth for all three versions of the Berlin-Brandenburg model at three different points in the models. The top left panels show the initial and calibrated temperature values or BB-LAB model and the stratigraphic columns for the points P1-P3. The top right panels show the same for the BB-6km model and the bottom panels for the BB-combined model. The bottom right panel shows the spatial position of the three points P1-P3.

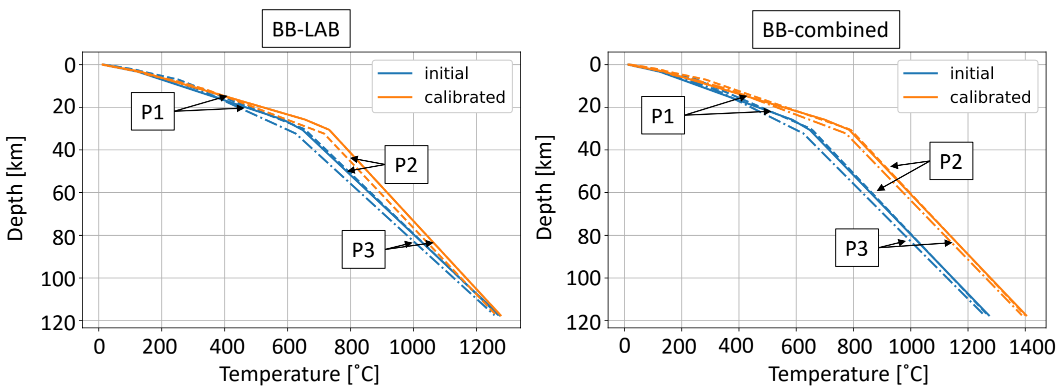

Figure 7. The left panel shows the calibrated and initial temperature distributions at the points P1-P3 for the BB-LAB model over the entire model depth. The right panel displays the initial and calibrated temperature distributions at the points P1-P3 for the BB-combined model over the entire model depth. For the positions of P1-P3 refer to Fig. 6.

stant for the former model. Although, we allow with a maximum temperature increase of 10 % a great amount of variation, the possible variations at a depth of 6 km are comparable to those of the Brandenburg 6 km model.

4.2.3 Approximation Quality and Computational Cost

Model	Forward Time FE [s]	Online time RB [s]	Speed-up	Time for SA [min]	Function evaluations SA	Number of basis functions	Rel. error tolerance
BB-LAB	73	$4\cdot10^{-3}$	$1.81\cdot10^{4}$	15.5	$2.8\cdot10^{5}$	248	$5\cdot10^{-4}$
BB-6km	526	$2\cdot10^{-3}$	$2.77\cdot10^{5}$	5.4	$2.4\cdot10^{5}$	143	$1\cdot10^{-3}$
BB-combined	501	$5\cdot10^{-3}$	$1.02\cdot10^{5}$	47.8	$3.0\cdot10^{5}$	273	$5\cdot10^{-4}$

Table 1. Summary of the computational cost for the global sensitivity analysis using the RB method.

We now briefly present the computational costs for the methodologies presented here (Tab. 1). For the BB-LAB and the BB-combined model, we defined a relative error tolerance of $5\cdot10^{-4}$ and for the BB-6km model a tolerance of $1\cdot10^{-3}$ for the model reduction. We reach these error tolerances in all cases (Fig. S1). Our most accurate measurements are 10^{-1} accurate, and the deepest measurement is at a depth of around 7 km. We chose these error tolerances to ensure that we do no introduce additional errors through the approximation in the entire model.

For the BB-LAB model, we require 248 basis functions to reach our pre-defined error tolerance. This leads to a reduction of compute time for a single forward simulation from 73 s to 4 ms. Hence, we have a speed-up of $1.81\cdot10^{4}$. Similarly, we require 143 basis functions to describe the BB-6km model and 273 for the BB-combined model (Fig. S1). Hence, we reduce the compute time for the BB-6km model from 526 s to 2 ms and for the BB-combined model from 501 s to 5 ms. Consequently, we obtain speed-ups of $2.77\cdot10^{5}$ and $1.02\cdot10^{5}$ for the BB-6km and the BB-combined model, respectively. The simulations for the speed-up have been performed on MacBook Pro (Intel Core i7, 2.5 GHz, 16 GB memory) using a single core. Using a physics-based machine learning approach resulted in compute times of 15.5 min (BB-LAB model), 5.4 min (BB-6km model), and 47.8 min (BB-combined model) for the Sobol sensitivity analysis with 280,000, 240,000, and 300,000 function evaluations, respectively.

4.3 Discussion

We demonstrated the dangers of constructing models with a low vertical depth. To further illustrate the importance of the placement of the lower boundary condition, we first discuss its impact by using the results of the global sensitivity study. Afterwards, we emphasize the consequences for inverse processes, by using a deterministic model calibration. Both analyses are presented for the case study of the Berlin-Brandenburg model.

4.3.1 Sensitivity Analysis

The impact of the lower boundary condition is apparent by focusing on the difference between the BB-6km, and the BB-LAB and combined models. For the Berlin-Brandenburg 6 km model, we fixed the boundary condition at 6 km depth, resulting in an entirely boundary dominated model. This is observable due to the enormous sensitivity of the model to the:

- Basement layer,
- scaling parameter of the respective boundary condition, and
- correlation between both parameters.

Consequently, all information that we obtain from the Brandenburg 6 km model is coming from the boundary condition. Hence, we have a model that is uninformative concerning the upper layers. However, these are the layers we are interested in since our target region is within these layers. Loosing the information about the thermal conductivities means that only the boundary is determining the solution. Hence, any errors of the boundary conditions have a possible huge impact on the temperature distribution at our target depth. This demonstrates that generating diffusive models with an extremely low vertical to horizontal length ratio is to be avoided at any cost.

The results of the global sensitivity analysis of the BB-LAB and combined model are matching our expectations. We observe a high sensitivity for the upper layers, which is caused by the shallow measurements (500 m to 6,820 m). First-order contributions of the Lower Cretaceous/Jurassic/Buntsandstein layers mostly impact the model. That means that the thermal conductivities of these layers are influencing the model themselves and not through a correlation with other layers. For the BB-LAB model, we combined the thermal conductivity of the Quaternary and the Tertiary layer into one training parameter. For the Brandenburg combined model, we combined the thermal conductivities of the Quaternary and Tertiary-post-Rupelian, and the Tertiary-pre-Rupelian-clay and Upper Cretaceous. Comparing the sensitivity analysis of both the BB-LAB model and combined model, we can conclude that the Tertiary-pre-Rupelian-clay is the layer that the model is sensitive to. We can rule out the Quaternary, and the Tertiary-post-Rupelian layer because the Berlin-Brandenburg combined model is insensitive to it. Furthermore, we can also eliminate the Upper Cretaceous because the Berlin-Brandenburg LAB model is insensitive to it. Also, the influence of the thermal conductivity of the Tertiary-pre-Rupelian-clay is mainly originating from the parameter itself and not from interactions between various parameters. Again, the influence of the Tertiary-post-Rupelian-clay seems counter-intuitive due to its low thickness. This influence is a combination of the shallow measurements, which lead to higher influences for the upper layers and the Dirichlet boundary condition at the top. This boundary conditions fixes the temperature for each evaluation to the same value, yielding a reduced influence of the Quaternary and therefore a relatively higher influence of the Tertiary layers.

Additionally, we get, for both models, a significant influence of the Lithospheric Mantle. Higher-order contributions dominate this parameter, and the second-order sensitivity indices show the parameter is correlated to the scaling parameter of the lower boundary condition. The Zechstein layer has similar influences in both model versions and is less significant in comparison to the overall influences.

To conclude, the only meaningful way to construct the model is by inserting the refined model into the original Berlin-Brandenburg LAB model. This results in the BB-combined model, which again shows the expected sensitivity distribution. One needs to keep in mind that this means an increase in degrees of freedom from 1,546,675 to 2,141,550. Nonetheless, both the finite element and the online execution time for both models are comparable since the complexity in these two models remains similar. This demonstrates that a reduction in the mathematical and not in the physical space is advantageous since it is much less restrictive.

4.3.2 Model Calibration

At first hierarchical model calibrations seem to be a way to transfer the knowledge from large-scale coarse models to smaller-scale fine discretized models. However, the sensitivities clearly show that the smaller model becomes uninformative towards the upper layers. That is especially dangerous because it is not noticeable looking at the temperature distributions at the observation points only. Hence, at a first glance, one would get to the conclusion that cutting-of the model at 6 km is a valid approach. However, this would only be possible if our sole interests are the temperatures at the measurement points used within the calibration. Naturally, a calibration will match the simulation to the observed temperatures. However, that comes at a cost. For the various model calibrations of the BB-6km model we obtain thermal conductivities ranging between 1.49 W m^{-1} K^{-1} and 2.83 W m^{-1} K^{-1} for the Basement layer. Meaning that we no longer have physical thermal conductivities but effective ones. These effective thermal conductivities are tailored to our measurements. However, if we are now interested in a different location (e.g. new drill-hole location), we can no longer derive reliable temperatures since our model calibration is not valid for this point and we lost the information about the physical system.

This brings us to the next important point. The above-described procedure is valid in a limited application field. However, one should be aware that the model is no longer representative of the physical processes. In contrast, both the BB-LAB and combined model have significant influences from various thermal conductivities. The lower boundary condition is further away from our target area, reducing possible effects from this condition.

In general, we want to improve through global SA the understanding of the physical model. In this specific case study, we demonstrate a way to determine the most influencing parameters allowing a back correlation to the geoscientific context. Note that we focus both the SA and the calibration on the observation locations. Hence, we observe higher influences of shallower layers. A study focusing solely on the temperatures at certain locations is applicable for some geophysical studies but if your interest goes beyond fitting the temperatures it is not advisable to use models that are cut-off at a shallow depth.

Note that we do not discuss the changes for the thermal conductivities in detail here. The reason is that we want to focus the discussion on the influence of the boundary condition. For further information about the thermal conductivities, we refer to the Supplementary Material S1.

4.3.3 Computational Cost

We presented an automated sensitivity-driven model calibration at the basin-scale. Considering that the global sensitivity analysis requires 280,000, 240,000, and 300,000 for the BB-LAB, BB-6km, and BB-combined model, respectively, it is clear that a model order reduction is needed to enable such an analysis. Using the reduced basis method showed extremely promising results because we obtain speed-ups of $1.81 \cdot 10^4$ to $1.65 \cdot 10^5$ without introducing approximation errors above the measurement error.

A comparison of the computational costs using the FE and RB method is summarized in Tab. 2. The offline stage of the Brandenburg combined model was computed on the RWTH compute cluster. We used two Intel Xeon Platinum 8160 CPUs (24 cores, 2.1 GHz, 192 GB of RAM), and it took 5.4 h. The other offline stages were computed on an Intel Westmere X675 machine (3.07 GHz 6 cores per chip, 12 cores per node and 24 GB memory per node). They required 2.9 h (Brandenburg LAB model) using 50 cores, and 57 min (Brandenburg 6 km model) using 48 cores. These time-consuming offline stages could be faster calculated using more cores. Nonetheless, the RB method is more efficient than the FE method because the offline stages contain up to 273 FE evaluations. This number is substantially lower than the number of function evaluations in this thesis. Note that we would have required 0.6 to 4.7 years for the Sobol sensitivity analysis using the FE problem one a single core. In contrast, we only required 5.4 min to 47.8 min using the RB method. Also, note the following, the forward evaluations are parallelizable, whereas most inversion routines are not. Additionally, the RB method allows on the fly adjustments of the parameters in the field, which is not possible for the full model.

Model	Time for SA using FE [a]	Time for SA using RB [h]	Offline Time [h]
BB-LAB	0.6	0.26	2.9
BB-6km	4.0	0.09	1
BB-combined	4.7	0.8	5.4

Table 2. Summary of the overall computational cost comparing the FE and RB method.

4.4 Outlook

Through this study, the path to subsequent tasks is opened. It would be interesting to further investigate the lower boundary condition. For some of the calibrations, we obtained very high thermal conductivities of the Lithospheric Mantle, which might be caused by the geometrical inaccuracies of the LAB. These inaccuracies would impact the lower boundary condition and the calibration would try to compensate for this by adjusting the thermal conductivity of the Lithospheric Mantle. We applied a scaling factor to the temperature value of this boundary to account for these inaccuracies, which slightly improved the results. However, a single parameter is not enough to compensate for the model errors. Therefore, we would like to replace the scaling factor by a function, which could be, for instance, determined through data assimilation. For this reason, an interesting next step to take would be to investigate if 3D-Var data assimilation yields improved results. In contrast to classical sequential data assimilation techniques, such as the Ensemble Kalman Filter (Burgers et al., 1998; Evensen, 1994), variational data assimilation is a continuous approach, where the entire time frame is considered. Variational data assimilation methods minimize a cost function to obtain an estimate of the state variable. Three dimensional variational data assimilation has been studied intensively in numerical weather forecast by, for instance, (Barker et al., 2004; Lorenc et al., 2000) but is fairly unknown for geothermal simulations. It has been studied in combination with the RB method already by Aretz-Nellesen et al. (2019). However, so far, the study is using benchmark problems only. Therefore, it would be interesting to investigate the performance of the method for complex geophysical problems.

Acknowledgments

We like to acknowledge Dr. Vera Noack for generating the Brandenburg model. Furthermore, we would like to acknowledge the funding provided by the DFG through DFG Project GSC111.

The temperature data used throughout this paper is available in Noack et al. (2012, 2013) and based on Förster (2001). For the construction of the reduced models, we used the software package DwarfElephant (Degen, Veroy, & Wellmann, 2020a). The software, which is based on the finite element solver MOOSE (Permann et al., 2020), is freely available on GitHub (`https://github.com/cgre-aachen/DwarfElephant`). The sensitivity analyses are performed with the Python library SALib (Herman & Usher, 2017).

References

Aretz-Nellesen, N., Grepl, M. A., & Veroy, K. (2019). 3D-VAR for parameterized partial differential equations: a certified reduced basis approach. *Advances in Computational Mathematics*, *45*(5-6), 2369–2400.

Barker, D. M., Huang, W., Guo, Y.-R., Bourgeois, A., & Xiao, Q. (2004). A three-dimensional variational data assimilation system for MM5: Implementation and initial results. *Monthly Weather Review*, *132*(4), 897–914.

Baroni, G., & Tarantola, S. (2014). A general probabilistic framework for uncertainty and global sensitivity analysis of deterministic models: A hydrological case study. *Environmental Modelling & Software*, *51*, 26–34.

Bayer, U., Scheck, M., & Koehler, M. (1997). Modeling of the 3d thermal field in the northeast german basin. *Geologische Rundschau*, *86*(2), 241–251.

Branch, M. A., Coleman, T. F., & Li, Y. (1999). A subspace, interior, and conjugate gradient method for large-scale bound-constrained minimization problems. *SIAM Journal on Scientific Computing*, *21*(1), 1–23.

Burgers, G., Jan van Leeuwen, P., & Evensen, G. (1998). Analysis Scheme in the Ensemble Kalman Filter. *Monthly weather review*, *126*(6), 1719–1724.

Cacace, M., Kaiser, B. O., Lewerenz, B., & Scheck-Wenderoth, M. (2010). Geothermal energy in sedimentary basins: What we can learn from regional numerical models. *Geochemistry*, *70*, 33–46.

Cannavó, F. (2012). Sensitivity analysis for volcanic source modeling quality assessment and model selection. *Computers & geosciences*, *44*, 52–59.

Cloke, H., Pappenberger, F., & Renaud, J.-P. (2008). Multi-method global sensitivity analysis (mmgsa) for modelling floodplain hydrological processes. *Hydrological Processes: An International Journal*, *22*(11), 1660–1674.

Degen, D., Veroy, K., Freymark, J., Scheck-Wenderoth, M., & Wellmann, F. (2020, Apr). Global sensitivity analysis to optimize basin-scale conductive model calibration - insights on the upper rhine graben. *EarthArXiv*. Retrieved from `eartharxiv.org/b7pgs` doi: 10.31223/osf.io/b7pgs

Degen, D., Veroy, K., & Wellmann, F. (2020a). Certified reduced basis method in geosciences. *Computational Geosciences*, *24*(1), 241–259. Retrieved from `https://doi.org/10.1007/s10596-019-09916-6` doi: 10.1007/s10596-019-09916-6

Degen, D., Veroy, K., & Wellmann, F. (2020b). Uncertainty quantification for basin-scale conductive models. *Earth and Space Science Open Archive ESSOAr*.

Ebigbo, A., Niederau, J., Marquart, G., Dini, I., Thorwart, M., Rabbel, W., ... Clauser, C. (2016). Influence of depth, temperature, and structure of a crustal heat source on the geothermal reservoirs of tuscany: numerical modelling and sensitivity study. *Geothermal Energy*, *4*(1), 5.

Evensen, G. (1994). Sequential data assimilation with a nonlinear quasi-geostrophic model using Monte Carlo methods to forecast error statistics. *Journal of Geophysical Research: Oceans*, *99*(C5), 10143–10162.

Fernández, M., Eguía, P., Granada, E., & Febrero, L. (2017). Sensitivity analysis of a vertical geothermal heat exchanger dynamic simulation: Calibration and error determination. *Geothermics*, *70*, 249–259.

Förster, A. (2001). Analysis of borehole temperature data in the northeast german basin: continuous logs versus bottom-hole temperatures. *Petroleum Geoscience*, *7*(3), 241–254.

Fuchs, S., & Balling, N. (2016). Improving the temperature predictions of subsurface thermal models by using high-quality input data. part 1: Uncertainty analysis of the thermal-conductivity parameterization. *Geothermics*, *64*, 42–54.

Gelet, R., Loret, B., & Khalili, N. (2012). A thermo-hydro-mechanical coupled model in local thermal non-equilibrium for fractured hdr reservoir with double porosity. *Journal of Geophysical Research: Solid Earth*, *117*(B7).

Herman, J., & Usher, W. (2017). Salib: an open-source python library for sensitivity analysis. *J. Open Source Softw*, *2*(9), 97.

Hesthaven, J. S., Rozza, G., Stamm, B., et al. (2016). *Certified reduced basis methods for parametrized partial differential equations.* SpringerBriefs in Mathematics, Springer.

Kastner, O., Sippel, J., Zimmermann, G., & Huenges, E. (2015). Assessment of geothermal heat provision from deep sedimentary aquifers in berlin/germany: A case study. *Assessment*, *19*, 25.

Kohl, T., Evansi, K., Hopkirk, R., & Rybach, L. (1995). Coupled hydraulic, thermal and mechanical considerations for the simulation of hot dry rock reservoirs. *Geothermics*, *24*(3), 345–359.

Lorenc, A., Ballard, S., Bell, R., Ingleby, N., Andrews, P., Barker, D., ... others

(2000). The Met. Office global three-dimensional variational data assimilation scheme. *Quarterly Journal of the Royal Meteorological Society*, *126*(570), 2991–3012.

Mottaghy, D., Pechnig, R., & Vogt, C. (2011a). The geothermal project den haag: 3d numerical models for temperature prediction and reservoir simulation. *Geothermics*, *40*(3), 199–210.

Mottaghy, D., Pechnig, R., & Vogt, C. (2011b). The geothermal project den haag: 3d numerical models for temperature prediction and reservoir simulation. *Geothermics*, *40*(3), 199–210.

Noack, V., Scheck-Wenderoth, M., & Cacace, M. (2012). Sensitivity of 3D thermal models to the choice of boundary conditions and thermal properties: a case study for the area of brandenburg (NE German Basin). *Environmental Earth Sciences*, *67*(6), 1695–1711.

Noack, V., Scheck-Wenderoth, M., Cacace, M., & Schneider, M. (2013). Influence of fluid flow on the regional thermal field: results from 3d numerical modelling for the area of brandenburg (north german basin). *Environmental earth sciences*, *70*(8), 3523–3544.

O'Sullivan, M. J., Pruess, K., & Lippmann, M. J. (2001). State of the art of geothermal reservoir simulation. *Geothermics*, *30*(4), 395–429.

Permann, C. J., Gaston, D. R., Andrš, D., Carlsen, R. W., Kong, F., Lindsay, A. D., … Martineau, R. C. (2020). MOOSE: Enabling massively parallel multiphysics simulation. *SoftwareX*, *11*, 100430. Retrieved from `http://www.sciencedirect.com/science/article/pii/S2352711019302973` doi: https://doi.org/10.1016/j.softx.2020.100430

Pribnow, D., & Clauser, C. (2000). Heat and fluid flow at the soultz hot dry rock system in the rhine graben. In *World geothermal congress, kyushu-tohoku, japan* (pp. 3835–3840).

Pribnow, D., & Schellschmidt, R. (2000). Thermal tracking of upper crustal fluid flow in the rhine graben. *Geophysical Research Letters*, *27*(13), 1957–1960.

Prud'homme, C., Rovas, D. V., Veroy, K., Machiels, L., Maday, Y., Patera, A. T., & Turinici, G. (2002). Reliable real-time solution of parametrized partial differential equations: Reduced-basis output bound methods. *Journal of Fluids Engineering*, *124*(1), 70–80.

Saltelli, A. (2002). Making best use of model evaluations to compute sensitivity indices. *Computer physics communications*, *145*(2), 280–297.

Saltelli, A., Annoni, P., Azzini, I., Campolongo, F., Ratto, M., & Tarantola, S. (2010). Variance based sensitivity analysis of model output. design and estimator for the total sensitivity index. *Computer Physics Communications*, *181*(2), 259–270.

Sippel, J., Scheck-Wenderoth, M., Lewerenz, B., & Klitzke, P. (2015). Deep vs. shallow controlling factors of the crustal thermal field–insights from 3d modelling of the beaufort-mackenzie basin (arctic canada). *Basin Research*, *27*(1), 102–123.

Sobol, I. M. (2001). Global sensitivity indices for nonlinear mathematical models and their monte carlo estimates. *Mathematics and computers in simulation*, *55*(1-3), 271–280.

Song, X., Zhang, J., Zhan, C., Xuan, Y., Ye, M., & Xu, C. (2015). Global sensitivity analysis in hydrological modeling: Review of concepts, methods, theoretical framework, and applications. *Journal of hydrology*, *523*, 739–757.

Tang, Y., Reed, P., Van Werkhoven, K., & Wagener, T. (2007). Advancing the identification and evaluation of distributed rainfall-runoff models using global sensitivity analysis. *Water Resources Research*, *43*(6).

Taron, J., Elsworth, D., & Min, K.-B. (2009). Numerical simulation of thermal-hydrologic-mechanical-chemical processes in deformable, fractured porous media. *International Journal of Rock Mechanics and Mining Sciences*, *46*(5), 842–854.

Turcotte, D. L., & Schubert, G. (2002). *Geodynamics*. Cambridge university press.

van Griensven, A. v., Meixner, T., Grunwald, S., Bishop, T., Diluzio, M., & Srinivasan, R. (2006). A global sensitivity analysis tool for the parameters of multi-variable catchment models. *Journal of hydrology*, *324*(1-4), 10–23.

Veroy, K., Prud'homme, C., Rovas, D. V., & Patera, A. T. (2003). A posteriori error bounds for reduced-basis approximation of parametrized noncoercive and nonlinear elliptic partial differential equations. In *Proceedings of the 16th aiaa computational fluid dynamics conference* (Vol. 3847, pp. 23–26).

Virtanen, P., Gommers, R., Oliphant, T. E., Haberland, M., Reddy, T., Cournapeau, D., . . . SciPy 1.0 Contributors (2020). SciPy 1.0: Fundamental Algorithms for Scientific Computing in Python. *Nature Methods*, *17*, 261–272. doi: 10.1038/s41592-019-0686-2

Vogt, C., Iwanowski-Strahser, K., Marquart, G., Arnold, J., Mottaghy, D., Pechnig, R., . . . Clauser, C. (2013). Modeling contribution to risk assessment of thermal production power for geothermal reservoirs. *Renewable energy*, *53*, 230–241.

Wainwright, H. M., Finsterle, S., Jung, Y., Zhou, Q., & Birkholzer, J. T. (2014). Making sense of global sensitivity analyses. *Computers & Geosciences*, *65*, 84–94.

Watanabe, N., Wang, W., McDermott, C. I., Taniguchi, T., & Kolditz, O. (2010). Uncertainty analysis of thermo-hydro-mechanical coupled processes in heterogeneous porous media. *Computational Mechanics*, *45*(4), 263.

Wellmann, J. F., & Reid, L. B. (2014). Basin-scale geothermal model calibration: Experience from the Perth Basin, Australia. *Energy Procedia*, *59*, 382–389.

Zhan, C.-S., Song, X.-M., Xia, J., & Tong, C. (2013). An efficient integrated approach for global sensitivity analysis of hydrological model parameters. *Environmental Modelling & Software*, *41*, 39–52.